RSC Advances

PAPER

View Article Online
View Journal | View Issue

Cite this: *RSC Adv.*, 2025, **15**, 42063

An unusual interlocked biomineral interface in bivalve shells

Jiaxi Huang and Gangsheng Zhang*

Bivalve ligaments are unusual biominerals that have evolved to facilitate the opening of the two shell valves when required. Over a long period of time, their microstructures have been well investigated and are generally considered to consist of an organic lamellar layer and an aragonitic fibrous layer (FL), where the fibers are mutually parallel with a uniform diameter of *ca.* 100 nm. However, the microstructure of the ligament-valve interface (LVI) has received little attention. Here, using optical microscopy, FE-SEM, powder XRD, and FTIR, we focus on the LVI's microstructure as well as its chemical composition in the clam *Cyclina sinensis*. We find that: (1) the LVI of this clam consists of discrete bands of coarse aragonite fibers with a variable diameter of 0.4–7.6 μm surrounded by fine aragonite fibers with a uniform diameter of 106.5 ± 1.6 nm; (2) these fine aragonite fibers are continuous with and similar in diameter to the FL fibers (116.8 ± 1.7 nm); and (3) the bands of coarse aragonite fibers penetrate the normal FL and gradually taper, bifurcate, or bend toward its interior, resulting in the LVI showing an unusual finger-joint-like microstructure. We propose that the LVI serves as a transition between the rigid valves and flexible normal FL and primarily functions to prevent the detachment of the FL from the valves during their movement, which could be caused by modulus mismatch between the flexible FL and the rigid valves. In short, this work provides a new model of biomineral interfaces, which may inspire the design and fabrication of advanced material interfaces.

Received 12th September 2025
Accepted 15th October 2025

DOI: 10.1039/d5ra06886j

rsc.li/rsc-advances

1 Introduction

Bivalve shells, such as oysters, mussels and clams, are natural biomineral materials, which usually consist of three basic parts: two rigid valves and an elastic ligament. The former mainly function as armor to protect the bivalve soft body, while the latter has at least two basic functions: (1) to hinge the two valves dorsally and (2) to open them ventrally when needed.[1] Therefore, both the valves and ligament are key biomineral tissues for the survival of bivalves.

Over a long period of time, both the valve and ligament have been extensively but separately studied due to their unique structures and superior mechanical properties. Now, it is well known that the valve may exhibit diverse structural patterns, such as prismatic, nacreous, or crossed-lamellar patterns, depending on the species.[2–4] In comparison, the ligament always contains only two patterns, which are called the lamellar and fibrous layer (FL), regardless of the species.[5–7] In particular, the FL always consists of aragonitic biomineral fibers embedded in a protein matrix.[8] These fibers are usually parallel to each other and show a convex polygonal or hexagonal shape in cross-section with a highly uniform diameter of *ca.* 100 nm.[9–12]

However, the ligament-valve interface (LVI) has been little investigated. To our knowledge, only two literature works concern the LVI. Carriker and Palmer[13] first reported that the oyster LVI (called the ligostracum) consisted mainly of aragonite prisms (diameter of *ca.* 4–6 μm). They proposed that this LVI in the oyster binds the organic ligament to the foliated calcite of the valve. Recently, Suzuki *et al.*[14] also noticed that the LVI (called the fusion interphase) in *Pinctada fucata* exhibits a prismatic structure that functions as a graded modulus transition zone between the ligament and nacre. Nevertheless, details about the microstructure of the LVI (such as the crystal orientation and spatial organization) and its precise function remain poorly understood.

Here, we investigate the microstructure and chemical composition of the LVI in *Cyclina sinensis* (Fig. 1), commonly known as the Chinese Venus clam, a species widely cultivated for human consumption along the southeastern coast of China. Interestingly, we observed a unique finger-joint-like microstructure formed by bands of coarse aragonite fibers penetrating the normal FL, which is common in this shellfish species. Moreover, we propose that the LVI serves as a clear connection between the rigid valve and elastic normal FL, primarily functioning to prevent detachment of the FL from the valves during their movement. Additionally, we briefly discuss the possible formation mechanism of the LVI.

Finally, in this work, the terminology describing the anatomical orientation of the ligament (or shell) follows

School of Resources, Environment and Materials, Guangxi University, Nanning, Guangxi 530004, China. E-mail: zhanggs@gxu.edu.cn

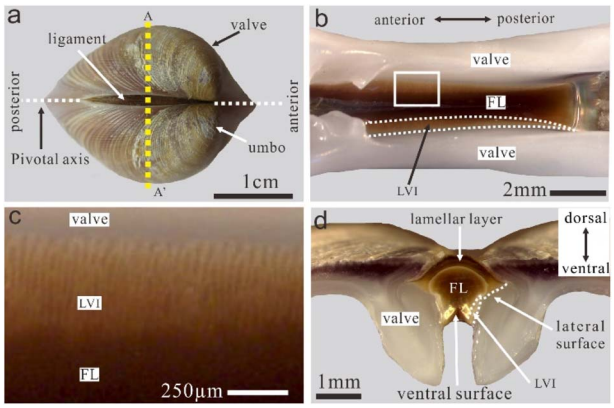

Fig. 1 Optical images of an intact *Cyclina sinensis* shell. (a) An outer (dorsal) view of the intact ligament. (b) An inner (ventral) view of the ligament. (c) An enlarged view of the boxed area from (b). (d) A transverse section cut perpendicular to the pivotal axis of the ligament (corresponding to a cut along the line AA′ from (a)). FL: fibrous layer; LVL: ligament-valve interface.

convention, as detailed by Trueman[6,15] and Fougerouse *et al.*[16] Particularly, the transverse section refers to the one cut perpendicular to the pivotal axis of the ligament (Fig. 1d). In addition, the cross-section refers to the one cut along the ventral surface of the ligament, and the lateral surface corresponds to the contact plane between the valve and ligament (Fig. 1d).

2 Materials and methods

The *Cyclina sinensis* clams were collected alive on the coast of Beihai City, Guangxi Province, southern China. They were processed as follows: (1) the soft tissues were removed from the shells with a scalpel; (2) the shells were cleaned with tap water followed by distilled water and air-dried at room temperature for 12 h; and (3) finally, using a single-sided blade, the samples were mechanically sectioned along different directions of the ligament.

For optical microscopy, the as-prepared sections of the ligament were first polished with 1000–6000-grit SiC paper and then observed with a stereo microscope (SZ66, Optec) equipped with a digital camera (GT5.0, Tucsen).

For chemical phase analysis, first, ligament fragments were scratched using a scalpel on the LVI of ligaments to obtain powdered samples. Then, powder X-ray diffraction (XRD) patterns were collected with a diffractometer (Bruker D8) using Cu K_α radiation ($\lambda = 0.15406$ nm) at 40 kV (200 mA). Finally, the powdered samples were mixed with KBr to obtain pellets, and their transmission FTIR (Fourier-transform infrared) patterns were collected with a spectrometer (Nicolet iS 50, ThermoFisher Scientific) at a resolution of 4 cm^{-1} with 32 scans in the range of 500–2000 cm^{-1}.

For SEM analysis, the as-prepared ligament sections were first coated with gold by a sputter coater (SBC-12, KYKY) operating under a vacuum of 6 Pa and at 6 mA for 30 s. Then, they were observed with FE-SEM (SU8020, Hitachi) operating at 10–30 kV. Finally, the SEM images were processed using quantitative image analysis software (QIA-64, Reindeer Graphics).

3 Results

3.1 Optical observations

Optical images of the *C. sinensis* shell are shown in Fig. 1. In general, the ligament of this species shows mirror symmetry along the pivotal axis of the shell (Fig. 1a and d). It looks like a thin lens when viewed from the outer surface (Fig. 1a) and an irregular rectangle when viewed from the inner surface (Fig. 1b). Interestingly, on the inner surface, there exists a thin transitional area between the FL and valve, namely, the LVI (Fig. 1b and c), which has a unique finger-like appearance. In addition, the LVI has a maximum thickness of *ca.* 0.5 mm for a 2.6-cm-long shell and tapers to the posterior end of the ligament. In the transverse section (Fig. 1d), the LVI looks like an oblique triangle tapering to the dorsal side, which will be detailed *via* the following SEM observations.

3.2 SEM observations

3.2.1 Transverse section. The transverse section cut through the ligament-valve contact area is shown in Fig. 2a, where three components exist: the FL, LVI, and valve (Fig. 2b). The former consists of parallel fibers with a highly uniform diameter of *ca.* 110 nm (Fig. 2c), which are usually slightly curved (Fig. S1) and similar in structure to the FL of other bivalves, as detailed elsewhere.[15,17,18] In contrast, the LVI exhibits an oblique triangular shape that tapers, with a maximum width of *ca.* 0.3 mm, and, located at the FL-valve interface, it has two distinct boundaries separating it from the FL and valve, respectively (Fig. 2b). Moreover, it consists of parallel fibers of highly non-uniform diameter (Fig. 2d), which can be divided into two types. One is called fine fibers, which are similar in diameter (*ca.* 120 nm) to those of the FL, and the other is called coarse fibers, which are highly non-uniform, ranging from *ca.* 1.7–4.8 μm. Interestingly, those two types of fibers are usually interpenetrating with no clear boundary. Their cross-sectional morphology will be detailed below.

The structure of the valve near the LVI surface consists of complex crossed-plate crystals with a thickness ranging from *ca.* 0.24–0.44 μm; these are significantly different in terms of orientation and diameter compared with the coarse fibers (Fig. 2e).

3.2.2 Cross-section. The cross-section through the FL and LVI areas and parallel to the ventral surface is shown in Fig. 3a. Specifically, the LVI is composed of alternating bands of fine and coarse fiber bands, and it has a thickness of *ca.* 160 μm (Fig. 3a and b). Notably, the fine fiber bands are composed of convex polygonal or hexagonal-shaped fibers in cross-section, which have a highly uniform diameter of 116.8 ± 1.7 nm, as determined by quantitative image analysis software (QIAs) (Fig. 3c and S2a). In addition, the normal FL is also composed of fine fibers with the same structure and a similar diameter (106.5 ± 1.6 nm) and shows no distinct boundaries separating the fine

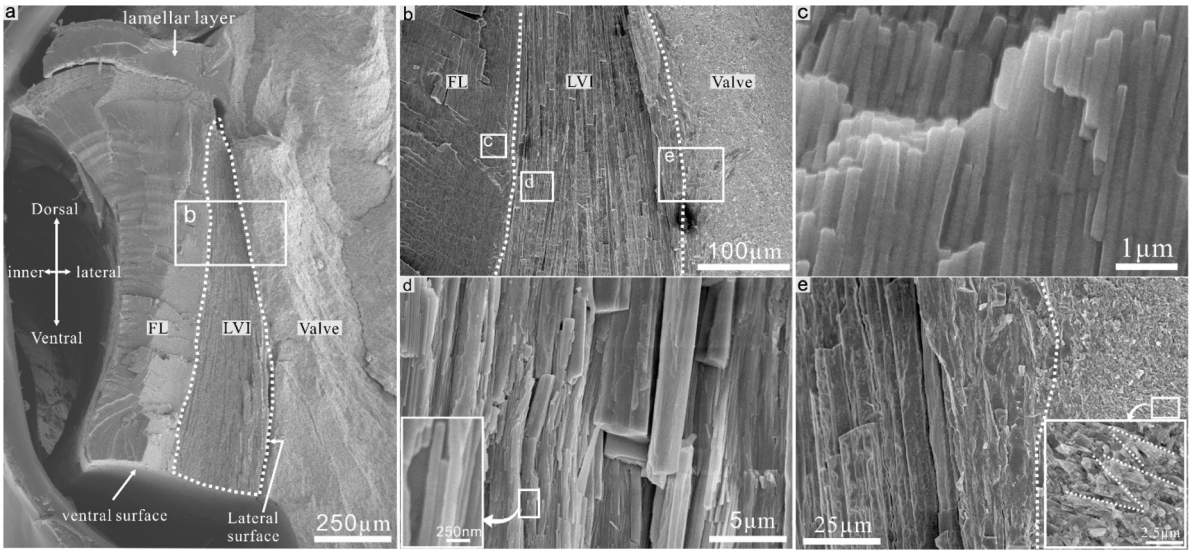

Fig. 2 SEM images of a transverse section of a portion of *C. sinensis* ligament cut along the line AA′ from Fig. 1a. (a) An overview of the ligament-valve contact area showing the location of the ligament-valve interface (LVI). (b) A close-up view of the boxed area b from (a). (c)–(e) Details of the boxed areas c–e from (b), respectively.

fiber bands (Fig. 3c and S2b). Therefore, the fine fiber bands are continuous with the normal FL.

In contrast, the coarse fiber bands have distinct boundaries separating them from the fine fiber bands (namely the normal FL), showing an abrupt transition between fiber types (Fig. 3b and e). Interestingly, we found that these coarse fiber bands penetrate the normal FL and gradually taper and bifurcate or bend towards the interior of the FL, with the width of the band ranging from *ca.* 5.6–14.1 μm (Fig. 3b and f). This results in an unusual finger-joint-like interlocked structure at the LVI. Moreover, the coarse fibers usually show a concave polygonal and highly non-uniform diameter (range: 0.4–7.6 μm; mean: 4.8 ± 0.2 μm) (Fig. 3d and S2c). This implies that the coarse fibers themselves form an interlocked structure within the bands.

3.2.3 Lateral surface. The lateral surface after the removal of the valve and lamellar layer is shown in Fig. 4a. Structurally, the LVI consists of bands exhibiting two different morphologies, coarse and fine fibers, on the lateral surface (Fig. 4b and e). In particular, we found that these fiber bands are composed of unique fan-shaped fiber bundles, with the fiber bundles approximately vertically aligned near the dorsal end of the LVI area (Fig. 4b and d). Moreover, within each bundle, the fibers

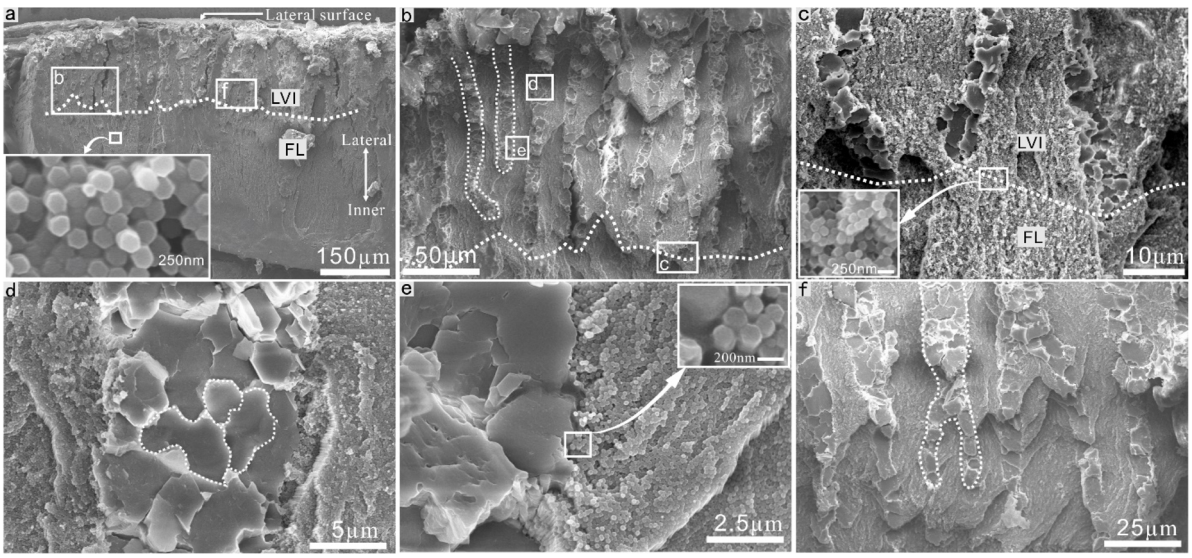

Fig. 3 SEM images of a portion of *C. sinensis* ligament and the LVI in cross-section. (a) An overview of the section where the top lateral surface corresponds to the contact surface with the valve. (b) A close-up view of the boxed area b from (a) with further details shown in (c), (d) and (e). (f) A close-up view of the boxed area f from (a).

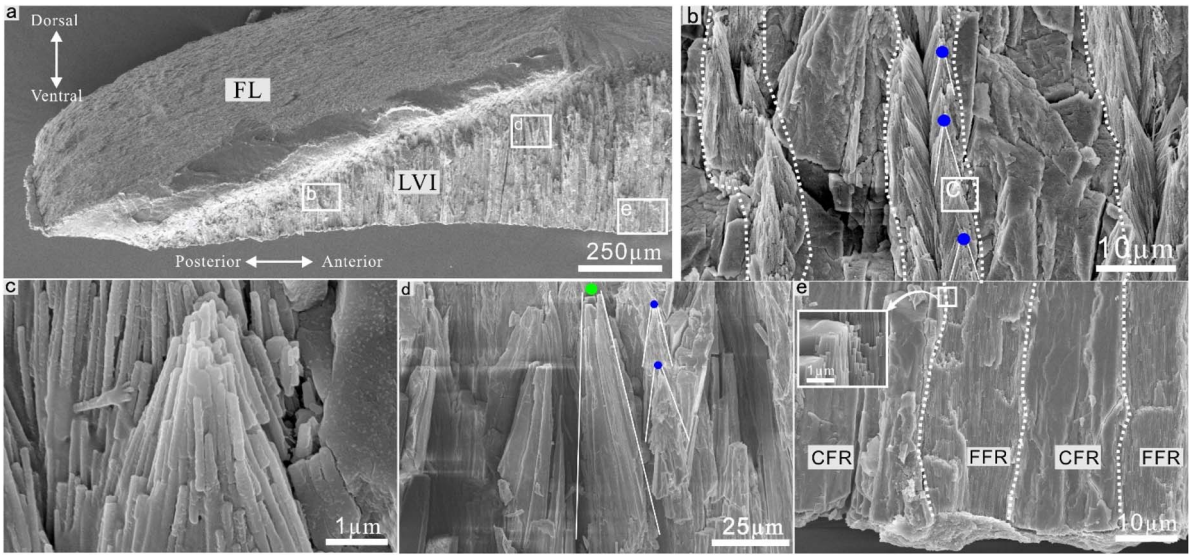

Fig. 4 SEM images of the lateral surface of a *C. sinensis* ligament. (a) An overview of the lateral surface. (b) A close-up view of the boxed area b from (a). (c) Details of the boxed area c from (b). (d) and (e) Close-up views of the boxed areas (d) and (e) from (a), respectively. The blue and green dots are predicted nucleation centers of the fine and coarse fiber bundles with a fan shape, respectively; CFR: coarse fiber; FFR: fine fiber.

converge at the nucleation center and divert in a ventral direction (Fig. 4c and d). This implies competitive growth between two neighboring fiber bundles near the dorsal end of the LVI area.[19–21]

In contrast, near the ventral end of the LVI area, the fibers within the bands are parallel to each other, and the coarse and fine fibers share the same orientation, with the widths of the coarse and fine fiber bands being 17.88 μm and 12.6 μm, respectively (Fig. 4e).

3.3 Chemical phase analysis

In the FTIR spectrum (Fig. 5a), the LVI showed characteristic aragonite peaks of CO_3^{2-} at 700 cm^{-1}, 713 cm^{-1}, 855 cm^{-1}, 1082 cm^{-1} and 1492 cm^{-1}.[22] In addition, the spectral signals at 1654 cm^{-1} (amide I) and 1401 cm^{-1} (symmetric CH_3 bending modes of the methyl groups of proteins) represent some characteristic peaks of organic materials.[23] In the XRD pattern (Fig. 5b), the LVI showed a series of sharp peaks that match well with those of aragonite (JCPDS file no. 05-0453).

EDS (energy dispersive spectroscopy) was used to analyze the coarse and fine fibers, respectively, showing that all these fibers contain C, O, and Ca, while the fine fibers also contain N and small amounts of S and Cl (Table S1). Among these, Ca, C, and O in the coarse fibers should originate from aragonite. In the fine fibers, Ca should originate from aragonite, C and O from both aragonite and organic materials, and the remaining elements from organic materials.

In summary, XRD and FTIR analyses confirm that aragonite is the only crystalline phase present in the LVI of *C. sinensis*. EDS results further indicate that the coarse fibers are composed of $CaCO_3$, while the fine fibers consist of $CaCO_3$ and organic

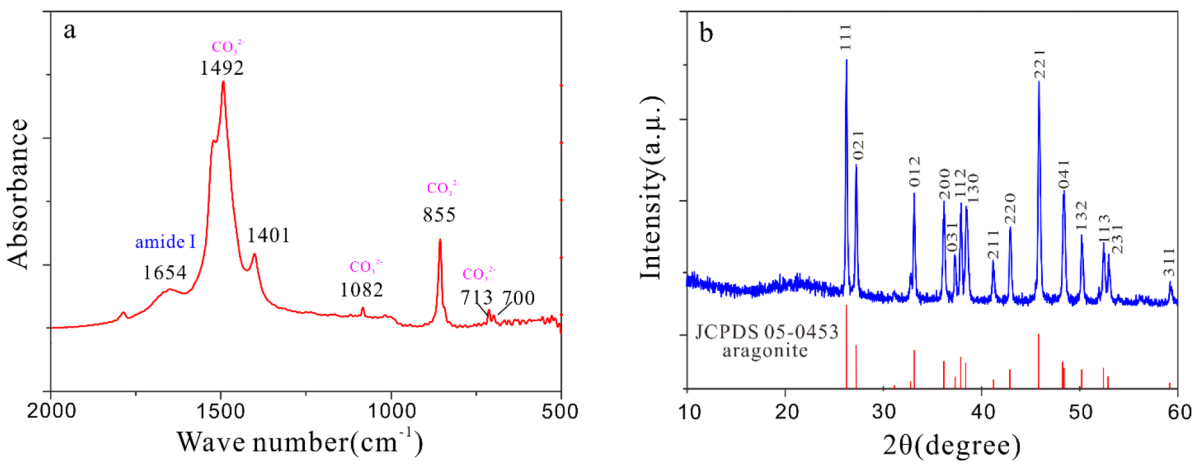

Fig. 5 FTIR (a) and XRD (b) patterns recorded from a powder sample of the LVI of *C. sinensis*.

material. Thus, the coarse fibers are predominantly aragonite, whereas the fine fibers comprise aragonite crystals and an amorphous proteinaceous matrix.

4 Discussion

4.1 Structural model of the LVI

Based on SEM observations of different sections, we could propose a structural model for the ligament-valve interface (LVI) of *C. sinensis* (Fig. 6). To clearly illustrate the location and structure of the LVI, half of the ligament tissue and part of the valve are removed, as shown in Fig. 6a. It is noteworthy that the LVI is an interlocked area formed by the penetration of the coarse fiber areas into the normal FL, located between the normal FL and the valve. In addition, the coarse fiber areas usually show a similar slender triangular pyramid shape in three-dimensional space. This leads to the LVI areas gradually widening from the dorsal surface to the ventral surface.

Moreover, the coarse fiber areas gradually taper and bifurcate or bend towards the interior of the FL when viewed from the ventral surface, where the coarse fibers usually show a concave polygonal shape and highly non-uniform diameter (Fig. 6b). Therefore, the coarse fiber areas exhibit a unique finger-joint-like interlocked structure in both the ventral view and in cross-section. In contrast, the fibers of the normal FL show a convex polygonal or hexagonal shape and highly uniform diameter. In addition, in the living state, the bivalve FL is always subject to a compressive force (F) exerted by the valves (derived from the adductor), and the FL undergoes a corresponding shape change.[24] The shape change of the FL will be detailed below.

4.2 Combination of the fibers of the LVI

The LVI of *C. sinensis* contains two types of fibers: coarse and fine aragonite fibers, as detailed above. The way in which these fibers combine is an important question, and it may be divided into three types: (1) the combination of fine fibers, (2) the combination of coarse fibers, and (3) the combination of coarse and fine fibers.

For type 1, the fine fibers should be connected by organic materials, based on the following evidence: (a) the FL contains of ~64% fine fibers and ~36% by volume of organic materials, based on QIAs (Fig. S5a and b), which is further evidenced by EDS and FTIR analyses, as mentioned previously; and (b) in slightly deformed areas of the FL, the fine fibers are directly observed to be joined by organic materials (red arrows in Fig. S4c).

For type 2, EDS analysis indicates that the bands of coarse fibers contain only C, O, and Ca, with no detectable N. This suggests an absence of an organic matrix at their boundaries. Therefore, the coarse fibers are likely in direct contact with each other along their interlocked zigzag boundaries (Fig. 3d and 6b).

For type 3, the coarse fiber bands are always surrounded by fine fibers, with an irregular boundary between them (Fig. 6b and S4d). Along the boundary, some extremely fine filaments are observed to join the fine and coarse fibers, which are probably organic materials.

4.3 Function of the LVI structure

SEM observations and EDS results indicate that the FL consists of fine aragonite fibers and organic material. It is well known that for a two-phase fibrous composite, its average elastic modulus can be estimated according to the rule of mixture:[25]

$$E_{FL} = E_a V_a + E_m V_m \quad (1)$$

where V_a and V_m ($=1 - V_f$) are the volume fractions of the fibers and matrix of the FL, respectively, and E_a and E_m are the elastic modulus values of the fiber and matrix, taken as 67–80 GPa and 0.16–0.26 GPa, respectively.[26,27] In addition, the fiber area fraction is ~64%, as determined by QIAs (Fig. S5a and b), which

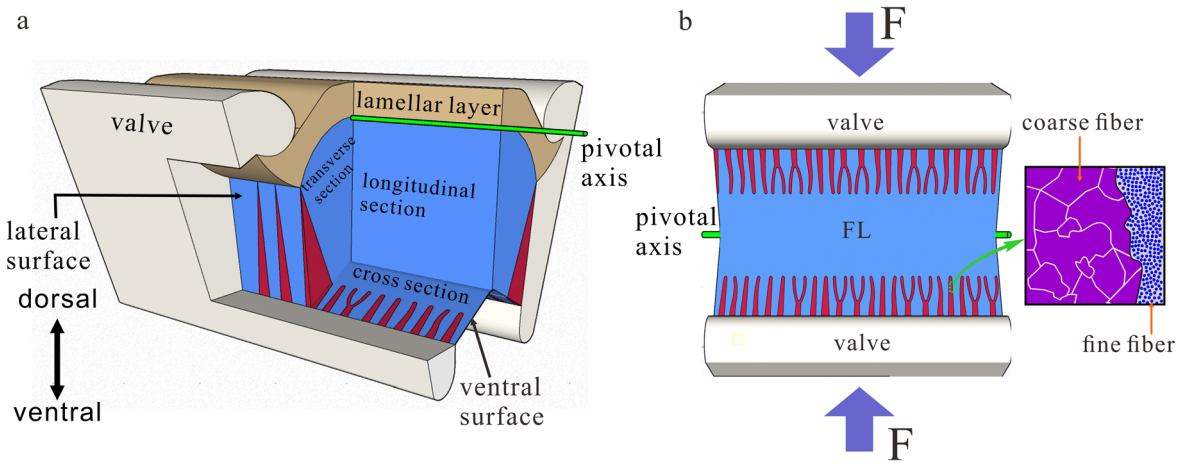

Fig. 6 Schematic diagrams of the ligament-valve contact area in *C. sinensis* shells viewed from different angles: (a) a perspective view, which shows the location and structure of the developed ligament-valve interface (LVI); and (b) a ventral view, which shows that the LVI consists of a finger-joint-like interlocked structure. Red areas: regions of coarse fibers; blue areas: regions of fine fibers. For simplicity, (1) parts of the ligament and valve are deliberately removed to show different sections of the ligament and the LVI; and (2) the orientations of both the coarse and fine fibers are neglected.

equals the fiber volume fraction (V_a), since the observed fracture surface is nearly perpendicular to the fiber axis. Correspondingly, the matrix volume fraction (V_m) should be ~36%. Therefore, the elastic modulus of the FL is ~47.12 GPa.

In contrast, the LVI consists of coarse fiber bands penetrating the normal FL, where the coarse fibers of the bands are likely in direct contact with each other. Thus, the elastic modulus of the LVI can be estimated according to the rule of mixture:

$$E_{LVI} = E_c V_c + E_{FL} V_{FL} \quad (2)$$

where V_c and V_{FL} (=1 − V_c) are the volume fractions of coarse aragonite fibers and the FL, respectively, and E_c and E_{FL} are the elastic modulus values of coarse fibers (since coarse fibers are aragonite, $E_c = E_a$) and the FL, respectively. In addition, the coarse fiber and FL volume fractions are ~25% and ~75%, respectively, as determined by QIAs. Therefore, the elastic modulus of the LVI is ~53.74 GPa.

Finally, the crossed-lamellar layer of the valve is composed of more than 99% aragonite with less than 1% organic matrix.[28] Its elastic modulus (E_V) is estimated as:

$$E_V = E_a V_{av} + E_m V_{mv} \quad (3)$$

where V_{ac} and V_{mv} (=1 − V_{ac}) are the volume fractions of aragonite and the organic matrix, respectively. Therefore, the elastic modulus of the valve is ~72.77 GPa.

Based on the calculated elastic moduli, a clear mechanical hierarchy is observed among the three structural components. The elastic modulus of the FL (~47.12 GPa) is substantially lower than that of the crossed-lamellar valve (~72.77 GPa), with a difference of approximately 27 GPa. Following conventional material classification based on the elastic modulus, the FL can be categorized as a relatively flexible or elastic material, whereas the valve exhibits the characteristics of a rigid material. Consequently, a critical problem arising at the connection between the flexible FL and the rigid valve is modulus mismatch. Specifically, the flexible FL deforms and elongates predominantly in the anteroposterior direction under compressive force, while the rigid valve experiences minimal elastic deformation. This subjects the LVI to shear stress resulting from the shape change of the flexible FL. Critically, the estimated modulus of the LVI (~53.74 GPa) is not uniform but represents the macroscopic mechanical properties of the structure as an integrated whole. Structurally, this modulus results from the characteristic structural configuration in which stiff coarse fibers (67–80 GPa) penetrate the compliant FL (~54.08 GPa). The elastic modulus of the LVI is ~53.74 GPa, positioned between the elastic moduli of the valve and FL. This provides crucial quantitative evidence for a mechanical gradient within the LVI, confirming that the interface functions as an integrated structure with transitional stiffness bridging the FL and the valve.

Therefore, based on structural observations, we propose that the LVI primarily functions to prevent the detachment of the FL from the valves during their movement. Specifically, the LVI achieves this function through at least two structural designs: (1) the finger-joint-like interlocked structure enhances the shear resistance of the LVI (Fig. 6b); and (2) the triangular pyramid structure design of the coarse aragonite fiber areas results in the elastic modulus of the LVI gradually increasing from the FL to the valve (Fig. 6a). Thus, this solves the modulus mismatch between the flexible FL and the rigid valve effectively.

In summary, the LVI serves as a transition between the rigid valve and the flexible normal FL and plays an important role in preventing ligament detachment. Unfortunately, we are unable to provide actual mechanical parameters, such as the elastic moduli of different parts, as further experiments such as nanoindentation are needed. This will be the direction of our future research.

4.4 Possible formation mechanism of the LVI

Based on the above observations, the most unique structure design of the LVI is the finger-joint-like interlocked structure formed by the coarse fibers penetrating the normal FL (Fig. 3). We propose a possible mechanism for the formation of this unique structure. This structure may form under compressive force from the adductor muscles. Specifically, an unstable connection exists between the flexible FL and the rigid valve at the growth end of the ligament, namely the posterior end of the ligament (Fig. 1b and 4). However, under compressive force, in regions where no finger-like structures are formed (namely the posterior end of the ligament), the FL undergoes deformation and elongates predominantly in the posterior direction, leading to finger-like fissure areas in the normal FL.

Based on SEM observations of the lateral surface, we propose a possible formation mechanism for the coarse fiber areas: random nucleation and competitive growth. Specifically, coarse fibers nucleate randomly on the valve surface and then grow randomly to the ventral direction, displaying fan-shaped spherulites (randomly symmetric aggregates of crystalline fibers that share a common growth axis but undergo branching with slight crystallographic deviations).[29,30] Within the finger-joint-like fissure areas, these fan-shaped spherulites then undergo competitive growth (Fig. 4d). The fibers compete for space, selecting the optimal orientation (perpendicular to the ventral surface). Consequently, only (or mainly) fibers with this orientation continue growing, ultimately forming parallel fibers (Fig. 4e).

In summary, the formation mechanism of the LVI likely involves two key stages. First, compressive forces deform the ligament at its posterior end and create finger-joint-like fissure areas. Subsequently, coarse aragonite fibers nucleate randomly on the valve surface, displaying fan-shaped spherulites, and undergo competitive growth within these fissure areas. This competitive selection favors fibers perpendicular to the ventral surface, which eventually grow into parallel fibers and form the interlocked structure of the LVI with the fine fibers.

4.5 Significance of this work

In this work, we focused on the LVI structure of *C. sinensis* and found the unique finger-joint-like interlocked structure of the

LVI. Based on SEM observations, we propose that the primary function of this structure is to prevent the detachment of the flexible FL from the rigid valves during their movement, addressing a critical failure point that would otherwise lead to bivalve mortality. Thus, we provide an organizational structural model of the LVI of *C. sinensis*. This model deepens our understanding of the interfacial function of bivalve biomaterials and provides direct bionic inspiration for rigid–flexible material interface optimization in engineering.

Crucially, the interlocked design offers exceptional resistance to interfacial fatigue failure – a major challenge in engineered composites. By distributing stresses efficiently across the joint and mitigating stress concentration at the rigid–flexible boundary, this bio-inspired architecture promises enhanced durability for applications requiring millions of cyclic loading cycles, such as in flexible electronics, soft robotics, and aerospace components.[31–33]

5 Conclusions

This work reveals for the first time the unique finger-joint-like interlocked microstructure at the LVI of *Cyclina sinensis*, formed by bands of coarse aragonite fibers (diameter: 4.8 ± 0.2 μm) penetrating the normal FL. This specialized interface effectively mitigates the modulus mismatch between the flexible FL and the rigid valves and prevents their detachment during valve movement, primarily through enhanced shear resistance and a graded modulus transition. The findings provide a novel biomineral interface model, offering significant inspiration for the design of robust and fatigue-resistant rigid–flexible integrated interfaces in advanced engineering materials.

Conflicts of interest

The authors declare that they have no known competing financial interests or personal relationships that could have appeared to influence the work reported in this paper.

Data availability

The authors confirm that the data supporting the findings of this study are available within the article and its supplementary information (SI). This file includes: Fig. S1: optical and SEM images of the longitudinal section. Fig. S2: histograms of particle size of fibers. Table S1: EDS (energy dispersive spectroscopy) analysis of the fine fibers and the coarse fibers with Fig. S3. Fig. S4: SEM images of the transverse-section of the ligament. Fig. S5: area diagrams of fine fibers and coarse fibers. See DOI: **https://doi.org/10.1039/d5ra06886j**.

Acknowledgements

We appreciate the financial support of the National Natural Science Foundation of China (Grant No. 41762004).

References

1 W. F. Ponder, D. R. Lindberg and J. M. Ponder, *Biology and Evolution of the Mollusca*, CRC Press, 2019, vol. 2, pp 55–132.
2 J. G. Carter, *Skeletal Biomineralization: Patterns, Processes and Evolutionary Trends Volume I*, Van Nostrand Reinhold, 1990.
3 M. S. Clark, L. S. Peck, J. Arivalagan, *et al.*, Deciphering mollusc shell production: the roles of genetic mechanisms through to ecology, aquaculture and biomimetics, *Biol. Rev.*, 2020, **95**(6), 1812–1837.
4 S. J. Eichhorn, D. J. Scurr, P. M. Mummery, M. Golshan, *et al.*, The role of residual stress in the fracture properties of a natural ceramic, *J. Mater. Chem.*, 2005, **15**, 947–952.
5 N. D. Newell and D. W. Boyd, *Iteration of Ligament Structures in Pteriomorphian Bivalves*, American Museum of Natural History, New York, N.Y., 1987, p. 11, ill., 26 cm.
6 *Treatise on Invertebrate Paleontology, Part N, Mollusca 6, Bivalvia 1*, ed. E. R. Ligament Trueman and R. C. Moore, Univ Kans Press, 1969, pp. 58–64.
7 T. R. Waller, The evolution of ligament systems in the Bivalvia, in *The Bivalvia*, ed. B. Morton, Hong Kong University Press, Hong Kong, 1990, pp. 49–71.
8 C. M. Yonge, Ligamental structure in Mactracea and Myacea (Mollusca: Bivalvia), *J. Mar. Biol. Assoc. U. K.*, 1982, **62**(1), 171–186.
9 W. H. Dall, *Contributions to the Tertiary Fauna of Florida, with Especial Reference to the Miocene Silex-Beds of Tampa and the Pliocene Beds of the Calooshatchie River*, 1895, vol. 3:3-4, pp. 1845–1927.
10 G. Bevelander and H. Nakahara, An electron microscope study of the formation of the nacreous layer in the shell of certain bivalve molluscs, *Calcif. Tissue Res.*, 1969, **3**, 84–92.
11 G. A. Kahler, R. L. Sass and F. M. Fisher, The fine structure and crystallography of the hinge ligament of *Spisula solidissima* (Mollusca: Bivalvia: Mactridae), *J. Comp. Physiol., B*, 1976, **109**, 209–220.
12 M. E. Marsh and R. L. Sass, Aragonite Twinning in the Molluscan Bivalve Hinge Ligament, *Science*, 1980, **208**, 1262–1263.
13 M. R. Carriker and R. E. Palmer, A new mineralized layer in the hinge of the oyster, *Science*, 1979, **206**, 692–693.
14 M. Suzuki, K. Kubota, R. Nishimura, *et al.*, A unique methionine-rich protein–aragonite crystal complex: structure and mechanical functions of the Pinctada fucata bivalve hinge ligament, *Acta Biomater.*, 2019, **100**, 1–9.
15 E. R. Trueman, The ligament of Tellina tenuis, *Proc. Zool. Soc. London*, 1949, **119**, 717–742.
16 A. Fougerouse, M. Rousseau and J. S. Lucas, Soft tissue anatomy, shell structure and biomineralization, in *The Pearl Oyster*, ed. P. Southgate and J. Lucas, Elsevier, 2008, pp. 77–102.
17 H. Zengqiong and Z. Gangsheng, A new structural model of bivalve ligament from Solen grandis, *Micron*, 2011, **42**(7), 706–711.
18 Z. Weigang and Z. Gangsheng, A humidity sensitive two-dimensional tunable amorphous photonic structure in the

bivalve ligament of Meretrix linnaeus, *J. Struct. Biol.*, 2015, **192**(3), 457–460.
19 T. Ubukata, Architectural constraints on the morphogenesis of prismatic structure in Bivalvia, *Palaeontology*, 1994, **37**, 241–261.
20 A. Rodriguez-Navarro and J. M. García-Ruiz, Model of textural development of layered crystal aggregates, *Eur. J. Mineral.*, 2000, **12**(3), 609–614.
21 A. Rodriguez-Navarro, Model of texture development in polycrystalline films growing on amorphous substrates with different topographies, *Thin Solid Films*, 2001, **389**(1–2), 288–295.
22 S. A. Bordenave, A. Badou, B. Gaume, *et al.*, Ultrastructure, chemistry and mineralogy of the growing shell of the European abalone Haliotis tuberculata, *J. Struct. Biol.*, 2010, **171**, 277–290.
23 Z. Movasaghi, S. Rehman and D. I. ur. Rehman, Fourier transform infrared (FTIR) spectroscopy of biological tissues, *Appl. Spectrosc. Rev.*, 2008, **43**(2), 134–179.
24 S. A. Wainwright, Stress and design in bivalved mollusc shell, *Nature*, 1969, **224**, 777–779.
25 K. Ramachandran, M. Khan, R. A. T. Perera, *et al.*, Tensile and flexural behavior of synthetic and hybrid natural fiber composites for lightweight applications, *Polym. Compos.*, 2025, **46**(Suppl. 1), S301–S313.
26 N. Zhang and Y. Chen, Nanoscale plastic deformation mechanism in single crystal aragonite, *J. Mater. Sci.*, 2013, **48**, 785–796.
27 C. F. Wählisch, *et al.*, Surviving the surf: The tribomechanical properties of the periostracum of Mytilus sp, *Acta Biomater.*, 2014, **10**(9), 3978–3985.
28 X. W. Li, H. M. Ji, W. Yang, *et al.*, Mechanical properties of crossed-lamellar structures in biological shells: A review, *J. Mech. Behav. Biomed. Mater.*, 2017, **74**, 54–71.
29 G. Lofgren, An experimental study of plagioclase crystal morphology; isothermal crystallization, *Am. J. Sci.*, 1974, **274**(3), 243–273.
30 A. D. Fowler, B. Berger, M. Shore, *et al.*, Supercooled rocks: development and significance of varioles, spherulites, dendrites and spinifex in Archaean volcanic rocks, Abitibi Greenstone belt, Canada, *Precambrian Res.*, 2002, **115**(1–4), 311–328.
31 C. Soutis, Fibre reinforced composites in aircraft construction, *Prog. Aero. Sci.*, 2005, **41**(2), 143–151.
32 D. H. Kim, N. Lu, R. Ma, *et al.*, Epidermal Electronics, *Science*, 2011, **333**, 838–843.
33 Y. A. AboZaid, M. T. Aboelrayat, I. S. Fahim, *et al.*, Soft robotic grippers: A review on technologies, materials, and applications, *Sens. Actuators, A*, 2024, **372**, 115380.